Sensors & Actuators: B. Chemical 414 (2024) 135892

Contents lists available at ScienceDirect

Sensors and Actuators: B. Chemical

journal homepage: www.elsevier.com/locate/snb

Tunable viscoelastic size-based particle separation in straight microchannels with triangular cross-sections

Eunhee Cho [1], Jeong-ah Kim [1], Mahmut Kamil Aslan, Yingchao Meng, Stavros Stavrakis [*], Andrew deMello [*]

Department of Chemistry and Applied Biosciences, Institute for Chemical and Bioengineering, ETH Zurich, Zurich, Switzerland

ARTICLE INFO

Keywords:
Viscoelastic focusing
Particle separation
Blood separation
Passive separation
Label-free separation
Triangular channel

ABSTRACT

In recent years, viscoelastic particle manipulation within microfluidic systems has received much attention due to the ease with which micron-sized objects may be maneuvered and isolated on the basis of size. While several factors, including both fluid and particle properties, regulate the precise locations and trajectories of micron-sized species flowing along a microchannel, the role of channel cross-section shape is critical, since it directly influences the fluid velocity profile and thus the direction and magnitude of hydrodynamic forces. It is therefore surprising that this parameter has not been comprehensively investigated for cell-based separations, especially since most viscoelastic microfluidic systems are only able to efficiently sperate cells over limited size ranges. To address this shortcoming, we present a viscoelastic microfluidic system integrating a triangular cross-section microchannel, for efficient and tunable size-based separations of micron-sized species. We find that particle focusing patterns can be controlled by simple variation of volumetric flow rates, which allows for the efficient separation of particles and cells of variable size. To showcase the efficacy of the approach, we present a size-based separation of various blood components, including white blood cells, platelets, and rare cells. By quantifying the number of particles collected at the outlets, we achieve recovery efficiencies of over 98%.

1. Introduction

The separation of suspended cells and particles from complex biofluids is an essential step in various biomedical applications [1]. The choice of separation technique depends on the properties (such as size, shape, and deformability) of the species of interest, the complexity of the biofluid, the required purity level, and the requirements of downstream analytics. Microfluidic systems are adept at manipulating, controlling, and processing small-volume fluid flows and have shown to be powerful tools for high throughput single-cell and single-particle manipulations [2,3].

Microfluidic platforms for the manipulation of micron-sized species can be categorized as being either active or passive in nature. Active methods, relying on magnetic [4], acoustic [5], electrophoretic [6], and optical [7] forces, have been successful in allowing selective particle separations. Whilst these approaches have been effectively utilized in separation applications, they require the use of complex equipment able to deliver stimuli in a user-defined manner. On the other hand, passive methods such as pinched flow fractionation (PFF) [8], microfiltration [9], deterministic lateral displacement (DLD) [10], hydrodynamic filtration [11], inertial microfluidics [12] and viscoelastic microfluidics [13], require minimal external instrumentation, whilst showing comparable separation efficiencies. Here, separation efficiency refers to the effectiveness of a method in isolating particles, for example based on their size, shape or charge. Prior to separation, particle focusing is typically performed, where species within a fluid flow are directed toward specific streamlines. Separation methods that leverage hydrodynamic forces, such as inertial or elastic lift forces, to manipulate particles or cells are of special interest [12–15]. Here, particle focusing is controlled by balancing different hydrodynamic forces within a flow to induce lateral migration of particles to equilibrium positions. Since hydrodynamic forces strongly depend on particle size, size-based separation can be achieved by controlling equilibrium focusing positions [12,13,15]. Simplicity of operation makes hydrodynamic focusing an extremely attractive option for applications requiring continuous and label-free separation [3]. Amongst passive methods, inertial

* Corresponding authors.
E-mail addresses: stavros.stavrakis@chem.ethz.ch (S. Stavrakis), andrew.demello@chem.ethz.ch (A. deMello).
[1] These authors contributed equally to this work and share first authorship

https://doi.org/10.1016/j.snb.2024.135892
Received 29 January 2024; Received in revised form 23 April 2024; Accepted 26 April 2024
Available online 3 May 2024

microfluidic systems are popular due to their high-throughput nature [16]. However, inertial systems are less suitable for separating bioparticles within complex biofluids since they may require additional processing steps, such as cell lysis [17] or whole blood dilution [18,19] to effectively isolate and separate desired bioparticles. In addition, high shear stresses are common in inertial systems due to the need to operate at high volumetric flow rates, which often results in cell damage or reduced viability [20,21]. For these reasons, cell manipulations within viscoelastic fluids have gained increasing attention as a route to separating/isolating rare cells from blood samples [22–25]. Here, (micron-sized) species manipulation is achieved by controlling both channel geometry and fluid rheology. Significantly, it has been shown that the use of fluid elasticity not only enables efficient manipulation of cells using simple fluidic geometries [26], but also allows for sheathless cell separation over a wide range of flow rates by simply modulating the rheological properties of the viscoelastic medium [27]. Importantly, viscoelastic microfluidic systems have been shown to be adept at manipulating nm-sized species [28–31], and separating biological species such as DNA, cells, viruses, bacteria and exosomes [13,32,33], since viscoelastic forces at low Reynolds numbers are effective at suppressing Brownian motion of small species [34].

Whilst several studies have investigated how hydrodynamic focusing is controlled by experimental parameters such as flow rate [35], viscosity [36], particle size [37] and shape [38], the role of channel cross-sectional shape on focusing has yet to be properly investigated. This is surprising, since channel cross-sectional shapes are known to play an important role in inertial microfluidic systems. For example, spiral, trapezoidal cross-section channels have been shown to modify the shape of Dean vortex cores close to the outer wall [39], allowing for enhanced separation efficiencies. Additionally, it is known that the use of non-rectangular channel cross-sections can be used to control inertial focusing positions [40–43]. For example, variation of the geometry of triangular cross-section channels can be used to modify both the number and location of focusing positions within inertial flows [42,43]. That said, such systems have yet to demonstrate efficient separation of various blood components and typically rely on image-based analysis of limited numbers of particles. In this regard, the use of viscoelastic separation schemes using triangular cross-section microfluidic channels is likely to offer a route to high efficiency cell separations. Interestingly, Kwon et al. [44] compared viscoelastic and inertial focusing in a rhombic cross-section channel, demonstrating (for various flow rates) "single-line" particle focusing along the channel centerline when using non-Newtonian fluids, and "double-line" focusing behavior when using a Newtonian fluid. Additionally, Raoufi and co-workers [45] utilized elasto-inertial focusing in trapezoidal, square, and circular channels to investigate the effects of cross-sectional geometry on the focusing process. Specifically, they showed that by changing the angle of a channel corner (trapezoidal - 50°, square - 90° and circular −180°) the direction of the viscoelastic force can be varied. For example, increasing the angle of the corner not only strengthens elastic forces, but also directs them towards the channel center. Subsequently, the same team investigated the focusing of micron-size particles using both Newtonian and viscoelastic fluids within various curvilinear microchannels (circular, rectangular and triangular). For Newtonian fluids in triangular cross-section channels, particles are primarily concentrated in the center of the channel, whilst in non-Newtonian fluids particle equilibrium positions shift towards the outer wall due to the synergistic effects of Dean and elastic forces [46].

Viscoelastic methods have recently been used to separate micron-sized particles [47,48], blood cells [49,50] and rare tumor cells [27,28,39,50–53]. Unfortunately, current strategies typically work for a limited range of particle sizes. Such limitations arise due to fixed critical cut-off sizes that are determined by channel geometries and dimensions and pose obvious challenges when dealing with samples containing particle species of variable size [54–56]. Indeed, most devices have a fixed design (that cannot be changed after fabrication) and work well only for a limited range of particle sizes. To address this issue, tunable particle separation methods, involving the alteration of fluid properties or flow rates, have been developed. For instance, Zhou et al. reported tunable particle/cell separations by adjusting both the viscosity of a polyethylene oxide (PEO) carrier fluid and the total flow rate [30]. By introducing different PEO solutions into a winding microfluidic channel, the authors were able to control the interplay between inertial lift, Dean, and elastic lift forces, giving rise to full control of equilibrium focusing positions. However, it should be noted that this approach struggles to efficiently separate both particle mixtures and heterogeneous human mesenchymal stem cells into the three component subpopulations. Additionally, Tian and co-workers reported tunable particle separations within a microfluidic co-flow by regulating the core-to-sample flow rate ratios [52]. Such an approach created two sharp interfaces between the co-flowing fluids, with large particles being able to penetrate the core PEO solution, leading to continuous and highly efficient particle separations. Nevertheless, it should be noted that the use of a guide flow to enhance separation efficiency significantly dilutes the concentration of particles/cells, resulting in reduced sample throughput.

Herein, and to overcome the aforementioned limitations, we present a viscoelastic microfluidic system for the sheathless isolation of blood components and rare cells from minimally (10-fold) diluted whole blood. With this microfluidic system, high-throughput and tunable size-based separations can be achieved. The device integrates a triangular cross-sectional microfluidic channel for particle focusing and three rectangular outlet channels to collect species of variable size. We first investigate the focusing of model particles with diameters between 3 and 10 μm as a function of volumetric flow rate, and show that excellent recoveries (>95%) and purities (>92%) can be realized. Subsequently, we use our microfluidic platform to separate platelets, red blood cells (RBCs), white blood cells (WBC) and rare cells from minimally (10-fold) diluted whole blood.

2. Material and methods

2.1. Fabrication of the microfluidic device

Microfluidic molds were fabricated on a silicon wafer by additive manufacturing using a Photonic Professional GT2 two-photon polymerization 3D printer (Nanoscribe GmBH, Stutensee, Germany). Polydimethylsiloxane (PDMS) (Elastosil RT 604 A/B Wacker, Munich, Germany) and curing agent were mixed thoroughly at a ratio of 10:1, poured onto the mold, and cured at 75°C for 30 minutes. The cured PDMS was then peeled from the wafer and holes for fluid inlets and outlets formed at the desired positions using a hole puncher (Syneo, West Palm Beach, USA). The PDMS device was then bonded to a 1 mm thick glass slide (76×26mm, Fischer Scientific AG, Switzerland) by exposing both surfaces to an oxygen plasma (EMITECH K1000X, Quorum Technologies, UK) for 1 minute at 1.7 mbar.

2.2. Viscoelastic carrier fluids

Three different concentration PEO solutions (0.2%, 0.6% and 1% w/v) were prepared in 1x phosphate buffered saline (PBS) at a pH of 7.4 (ThermoFisher, Zug, Switzerland). All solutions were aged in the dark for at least one month before being used. The final viscosities of each solution were measured by an MCR-302 rheometer (Anton Paar, Graz, Austria) and are shown in Figure S1.

2.3. Particle and cell samples

Polystyrene (PS) particles having average diameters of 3 μm, 7 μm or 10 μm (Sigma-Aldrich, Buchs, Switzerland), were used as proxies for platelets, RBCs and WBCs, respectively. Particles were dispersed in aqueous solutions of PEO (Sigma-Aldrich, Buchs, Switzerland). Blood samples were obtained from the Zurich Blood Donation Center

(Blutspende SRK, Zurich, Switzerland). Before each experiment, blood samples were diluted 10-fold, and their rheological properties were modified by the addition of PEO. For all experiments involving blood samples this was achieved using a 0.3% PEO solution (instead of a 0.6% PEO solution) so as to match the rheological profiles observed in the corresponding particle experiments. For "rare cell" separation experiments, HEK293T Flp-in T-REX cells (ThermoFisher, Zurich Switzerland) were spiked into the diluted blood sample at a ratio of 1:10,000. These cells, expressed with a stably integrated mNeonGreen transgene (293 T Flp-in T-REX mNeonGreen: Dr. Mateescu, University Zürich) were cultured in DMEM medium (Life Technologies, Zug, Switzerland), supplemented with Glutamax (Life Technologies, Zug, Switzerland), 10% (v/v) fetal bovine serum (Life Technologies, Zug, Switzerland) and 1% (v/v) Penicillin-Streptomycin (10,000 U/mL, Life Technologies, Zug, Switzerland) inside a Galaxy 170 S incubator at 37°C and 5% CO_2, (Eppendorf, Schönenbuch, Switzerland). All experiments were performed with cells in their exponential (log) phase of growth. Two days before each experiment, 6 million cells were seeded in a 10 cm culture plate (Sigma-Aldrich, Buchs, Switzerland) in the presence of 2 μg/mL doxycycline (Sigma-Aldrich, Buchs, Switzerland) to induce expression of the mNeonGreen protein. Subsequently, adherent cells were trypsinized, and the corresponding cell suspension washed once in PBS before resuspension in PBS supplemented with 5% (v/v) fetal bovine serum to a concentration of 3 million cells per mL.

2.4. Microfluidic device operation

Solutions containing either particles, cells or blood were transferred to a 1 mL Plastipak syringe (BD, Eysins, Switzerland) and injected into the microfluidic device using a NEMESYS syringe pump (CETONI, Korbussen, Germany). 250 μm i.d. Tygon tubing (Tygon®S-54-HL, Fisher Scientific, Reinach, Switzerland) was used to connect syringes to the inlets and outlets of the microfluidic device. Cell suspensions inside the syringes were manually stirred using a 2 ×5 mm magnetic bar (VWR, Schlieren, Switzerland) to prevent sedimentation and ensure delivery of a uniform cell suspension. The microfluidic device was mounted on an inverted Eclipse Ti-E microscope (Nikon, Zurich, Switzerland) equipped with an IDT MotionPro Y5.1 high-speed camera (Videal, Niederönz, Switzerland) and a 20X, 0.45 NA S Plan Fluor objective (Nikon, Zurich, Switzerland). Suspensions of particles at different 1MDa PEO concentrations (0.2%, 0.6% and 1% (w/v)) were injected into the microfluidic device and their viscoelastic focusing trajectories were investigated at volumetric flow rates between 200 μl/hr and 800 μl/hr. Focusing positions were determined from brightfield images using an in-house MATLAB (MathWorks, Natick, Massachusetts, USA) routine implementing the Circle Hough Transform algorithm.

2.5. Evaluation of separation performance

To evaluate separation performance, samples collected from each outlet were analyzed using a Cytoflex S flow cytometer (Beckman Coulter, Brea, USA). Forward scatter (FSC) and side scatter (SSC) signals (488 nm excitation) were used to assess particle/cell size. SSC signals originating from RBCs and WBCs were distinguished by using 405 nm excitation, since hemoglobin in RBCs absorbs strongly at this wavelength [57]. Fluorescence emission from HEK293T cells expressing mNeonGreen allowed their discrimination from other blood cells. Flow cytometric data were processed using Flowjo V 10.8.0 software (BD Biosciences, Allschwil, Switzerland). Recovery and purity values were calculated using the number of cells counted by flow cytometry analysis. Specifically, purity was defined as the ratio of the number of target species at the target outlet(s) to the total number of species exiting at the target outlet. Recovery was defined as the ratio of the number of target species collected from the target outlet to the total number of target particles exiting the device. Additionally, the RBC rejection ratio (defined as the number of RBCs collected from the center outlets to the number of RBCs collected from all outlets) was used as a proxy for recovery when analyzing small numbers of cells in dilute blood samples.

2.6. Characterization of the viscoelastic fluid using dimensionless numbers

The Reynolds number (*Re*) and Weissenberg number (*Wi*) were used to characterize the viscoelasticity of PEO solutions. *Re* assesses the ratio of inertial to viscous forces, and is given by

$$\mathrm{Re} = \rho U D_h / \eta$$

where ρ is the density of the fluid, η the dynamic viscosity, U the average flow velocity and D_h the hydraulic diameter of a microchannel. For a triangular (isosceles) cross section D_h is given as

$$D_h = 2wh/(w + 2\delta)$$

where w and h are the width and height of the triangular channel respectively and δ is the length of the side walls of the triangular channel. The side walls refer to the two inclined planes that form the sides of the triangular channel. *Wi* characterizes the relative importance of elastic forces with respect to viscous forces and is defined as the product of the relaxation time, λ, of a fluid and the average shear rate $\dot{\gamma}$ of the fluid flow over the channel cross section, i.e.

$$Wi = \lambda\dot{\gamma} = 2\lambda U/D_h$$

η values were extracted from the plot of viscosity versus shear rate, as shown in Figure S1, with λ values for 1MDa PEO solutions being taken from the literature [58]. This analysis yielded $\eta = 5.1$ mPa.s and $\lambda = 0.0005$ s for a 0.2% (w/v) PEO solution, $\eta = 14.8$ mPa.s and $\lambda = 0.0011$ s for a 0.6% (w/v) PEO solution and $\eta = 44.5$ mPa.s and $\lambda = 0.0048$ s for a 1% (w/v) PEO solution. All experiments were conducted at *Re* values between 0.11 and 0.78, and *Wi* values between 9.23 and 64.04. When $Re < 1$ and $Wi > 0$, inertial forces are dominated by viscoelastic forces. In the present case, the 0.6% PEO exhibits apparent shear-thinning viscosity, as depicted in Figure S1. Consequently, at sufficiently high velocities (shear rates $>3000\ s^{-1}$) as employed in the microfluidic experiments, we assume that the mean viscosity of the 0.6% PEO solution corresponds to its highest shear viscosity recorded in Figure S1. Thus, for the aqueous 0.6% PEO solution, the shear viscosity is determined to be 8.15 mPa s.

3. Results

3.1. Geometrical and operational features of the viscoelastic microfluidics platform

A schematic of the microfluidic device and the principle of size-based particle tunability are shown in Fig. 1. The device comprises an inlet, a triangular cross-section channel, and an expansion channel of variable height integrating three outlet channels. Our microchannel design was based on a design reported previously for inertial separations [42]. We modified the parameters used in this work, including the apex angle and the large channel width while maintaining the length of 3.5 cm. We also modified the channel height from 88 μm to 15 μm. This adjustment was made to minimize the difference in focusing positions between particles with diameters of 7 μm and 10 μm. Our design uses a straight triangular cross-section channel (120 μm wide, 15 μm high, 35 mm long, with an apex angle of 152°) to focus micron-sized particles or cells. This was followed by a separation unit that fractionates particles based on their size (Figure S2). This unit, which directs particles towards the different outlets, features three rectangular cross-section channels all having a channel height of 15 μm. The fluidic resistance of each outlet was adjusted to increase the separation efficiency. Notably, the expansion structure of the central outlet unit incorporates a larger width compared

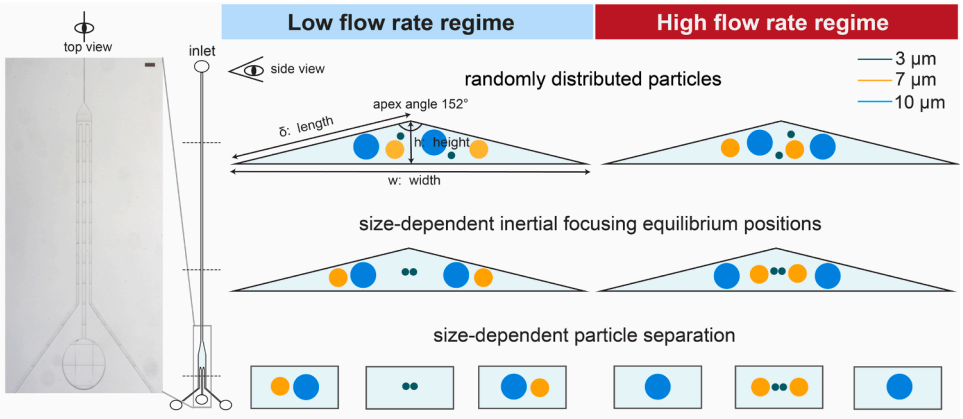

Fig. 1. Tunable size-based separation using a microfluidic triangular channel. The microfluidic device features an inlet, a straight microchannel (length: 35 mm) with a triangular cross-sectional shape (width: 120 μm, height:15 μm, apex angle: 152°) and a separation zone with three outlets (inset). Illustrations of the channel cross sections at different regions of the device (inlet, focusing and sorting regions) depicting the corresponding particle distributions. At low flow rates, 3 μm (dark green) particles are focused at the center, while 7 μm (orange) and 10 μm (cyan) particles are focused near the side walls. Consequently, the 3 μm particles can be purified from the particle mixture and collected at the center outlet, while the 7 and 10 μm particles are collected from the side outlets. As flow rate increases, focusing positions of 7 μm particles are altered from side walls to the centerline. Thereby, the remaining 10 μm particles are purified from the side outlets, while the 3 μm and 7 μm particles are collected from the center outlet.

to the other outlets to minimize flow resistance. In general, when using viscoelastic carrier fluids, both inertial and viscoelastic effects control particle migration. Specifically, three hydrodynamic forces (the elastic force, F_E, the inertial lift force, F_L, and the drag force, F_D) act on contained particles [47], providing control over both particle trajectories and equilibrium positions. If the elastic and inertial forces are comparable, 3D focusing at the center of the channel can occur. This balance establishes equilibrium positions for particles within the flow, resulting in their alignment along the centerline of the channel. Particles will migrate to the center of the channel due to the elasto-inertial effect [59], with the speed of lateral migration being proportional to the particle size. By pre-aligning species of different sizes in the triangular cross-section microchannel, size-dependent lateral migration can be subsequently induced in the expansion zone, creating a lateral separation between species of different size.

In the current system, size-based separation can be understood through the balance between F_L and F_E induced by the viscoelastic carrier fluid. F_L consists of two components: the shear-gradient lift force and the wall induced lift force. The wall induced lift force increases inversely with the normalized distance of the particle from the wall, and thus the magnitude of the wall-induced lift force is much larger than the shear gradient lift force [12,16,37] in situations where particles are relatively close to the channel walls, with the latter becoming increasingly insignificant when Re is small ($Re<1$). Given that inertia is non-negligible in the Re range used in the current study ($0.11 < Re < 0.78$), the combined effects of the wall-induced lift force ($F_{WL} \sim \rho U^2 a^6/H^4$, where H the channel dimension and a the particle diameter) [12, 16] and the elastic force ($F_E \sim \lambda(a/w)^3 Q^3$, where w the channel width, and Q the volumetric flow rate) [13,36] will determine the focusing trajectories [53]. It should be noted that the magnitude of both forces increases with increasing particle size and volumetric flow rate.

Recently, it has been shown that a triangular cross section channel displays unusual inertial particle focusing behavior due to the unique velocity profile [42]. As noted previously, there exists a significant difference in the behavior of wall-induced lift forces ($\propto a^6$) and elastic forces as a function of flow rate. Specifically, wall-induced lift forces grow more quickly compared to elastic forces as particle size is increased, leading to off-center focusing positions. Conversely, elastic forces are more sensitive to flow rate variations than wall-induced lift forces, with increasing flow rates causing particle positions to shift towards the centerline. Accordingly, it is critical that both factors be considered when designing and optimizing particle separation platforms.

3.2. *The effect of elasticity and flowrate on viscoelastic focusing*

To investigate the effects of elasticity on particle migration, experiments were carried out using three different particle sizes and volumetric flow rates ranging between 200 and 800 μl/hr. We initially investigated the effect of PEO concentration on particle focusing behaviour across the channel (Figure S3), using 7 μm diameter particles and PEO concentrations between 0.2% and 1%. For all PEO concentrations studied, changes in flow rate led to variations in focusing positions. Most notably, for the 0.6% PEO carrier fluid, an increase in the flow rate from 200 μl/hr to 800 μl/hr moves the two particle streams from close to the channel walls to close to the centerline. For this reason, a PEO concentration of 0.6% was used in subsequent experiments. Fig. 2 shows the focusing behaviour of three different particle populations suspended in a 0.6% PEO solution at flow rates between 200 and 800 μl/hr. Fig. 2**a** presents particle trajectories for each particle diameter/flow rate combination, demonstrating the tuning of particle focusing positions. Corresponding focusing position distributions are shown in Fig. 2**b**. Here, particle positions are normalized by channel width, with the channel center being located at 0 and the channel walls at ± 0.5. At all flow rates, 3 μm diameter particles, are focused to a single stream at the channel center, whilst a tiny fraction remains close to the channel walls at low flow rates (Fig. 2, **left**). Conversely, at low flow rates (200 μl/hr), both 7 μm and 10 μm diameter particles (Fig. 2, **middle and right**) travel in two equivalent streams that are distal to the channel center. 7 μm diameter particles are focused slightly closer to the side corners of the channel, as they experience a lower wall-induced lift force ($F_{WL} \sim \rho U^2 a^6/H^4$) than the 10 μm diameter particles. Additionally, the addition of F_E (which scales with U^3 and a^3) tends to push the 10 μm diameter particles towards the center of the channel, with the minimum shear rate due to the viscoelastic Poiseuille flow. For 7 μm diameter particles, when the volumetric flow rate is increased to 500 μl/hr, two additional flows appear at intermediate axial positions. At the highest flow rate (800 μl/hr), these trajectories converge, with all particles being located within 20 μm of the centerline. For all volumetric flow rates up to 800 μl/hr, the 10 μm diameter particles move in two equivalent trajectories located approximately 20 μm from the centerline (Fig. 2, **right**). Additional increases in volumetric flow rate above 800 μl/hr cause these trajectories to converge progressively closer to the centerline (Figure S4). These data confirm that particle focusing positions in a non-Newtonian

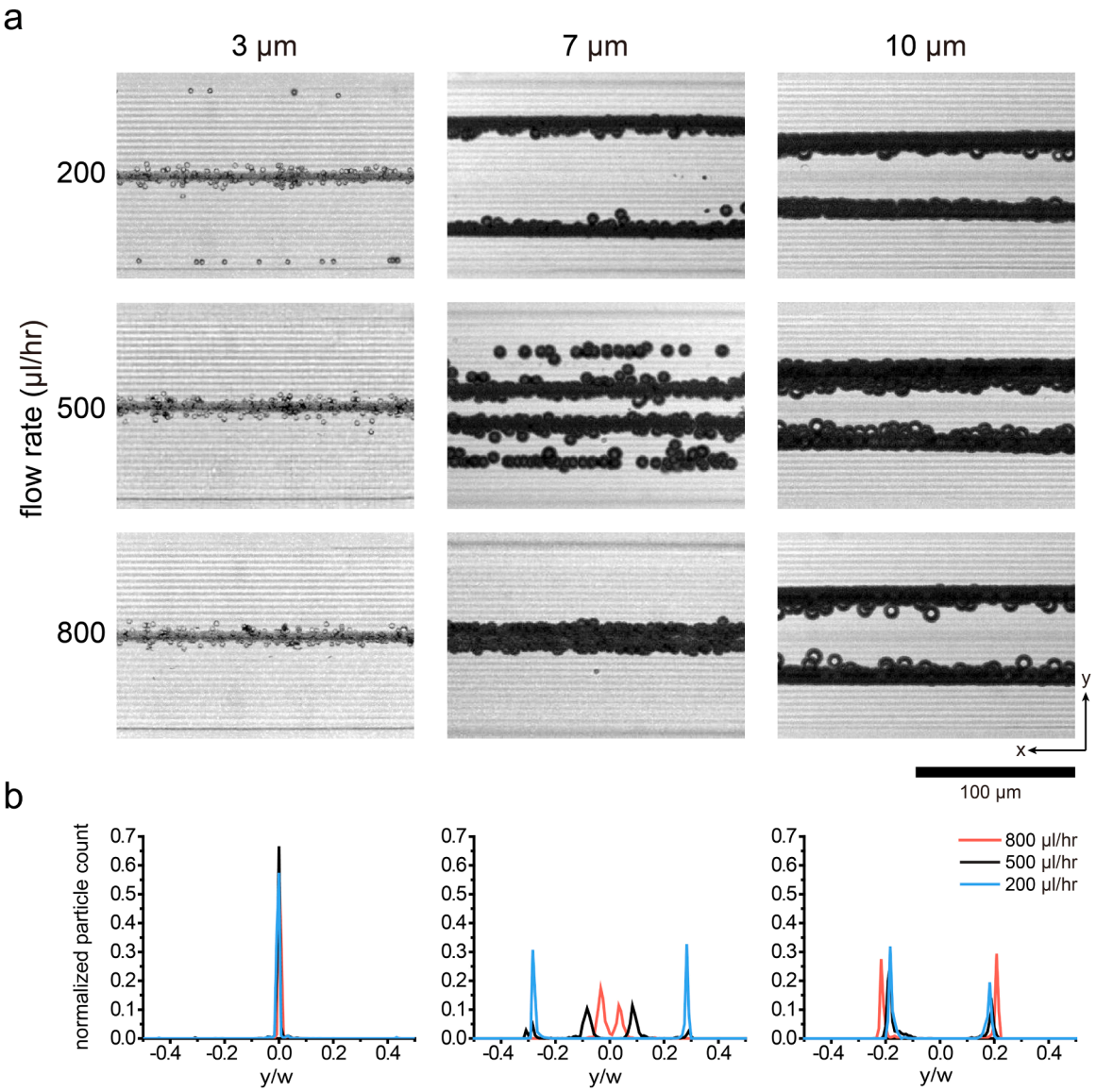

Fig. 2. Efficient tuning of the focusing positions of different particle sizes (3 µm, 7 µm, 10 µm). Particles suspended in a 0.6% w/v PEO solution were flowing in a channel of 120 µm width and 15 µm height. Image stacks of the focusing particle trajectories at 200, 500 and 800 µl/hr flow rates (a) and histograms showing the corresponding particle distributions across the channel in the y-direction (b). Both (a) and (b) show the dependence of viscoelastic focusing on the flow rates. 3 µm particles (left panel in a and b) have a single focusing position at the channel center that remains unchanged upon variation of the flow rate. On the other hand, the two streams of 7 µm particles (middle panel in a and b) located near the side walls at 200 µl/hr are starting to shift toward the channel center when the flow rate is changed to 500 µl/hr. In the case of 10 µm particles the two streams (right panel in a and b) remain between the center and the side walls at 200, 500 and 800 µl/hr flow rates. The particle distributions are normalized by dividing the number of particles to the channel width (w), and the bin size of the histogram is 1 µm.

fluid shift toward the channel center plane with increasing flow rate. Moreover, significantly higher flow rates are required to change the trajectories of larger particles compared to smaller particles. Such an interplay between volumetric flow rate and particle size can in principle be leveraged to allow for efficient and passive size-based separations of micron-sized species.

In general, we observed that at the lowest volumetric flow rate (200 µl/hr, $Re = 0.11$, $Wi = 9.23$), the focusing trajectories of the 3 µm particles are close to the channel centerline, whereas 7 µm and 10 µm diameter particles are focused near the side walls but at different heights. At higher flow rates (800 µl/hr, $Re = 0.45$, $Wi = 37.23$), 3 µm and 7 µm diameter particles travel close to the centerline, whilst 10 µm diameter particles remain closer to the channel walls until the flowrate exceeds 1400 µl/hr. Consequently, switching of the 7 µm particle focusing positions by volumetric flow rate variation acts as an effective route to particle separation, since 7 µm particles that lie near the sidewalls at low flow rates, shift towards the centerline as flow rate is increased.

3.3. Particle separation via tunable viscoelastic focusing

To evaluate the performance of the platform for tunable particle separation, we measured the composition of fluid at the inlet and each of the three outlets using flow cytometry. Fig. 3**a** presents a plot of side scatter area (SSC-A) vs forward scatter area (FSC-A) for an initial mixture of 3 µm, 7 µm and 10 µm particles. Analysis indicates that the initial sample comprised 33.3%, 49.3%, and 17.4% of the 3 µm, 7 µm and 10 µm particles, respectively. As noted, separation was performed using a flow rate of either 200 µl/hr or 800 µl/hr. Fig. 3**b** shows an image stack of particles at 200 µL/hr in the region where the triangular channel meets the expansion zone. It can be observed that under these conditions the 3 µm particles focus close to the channel centerline and

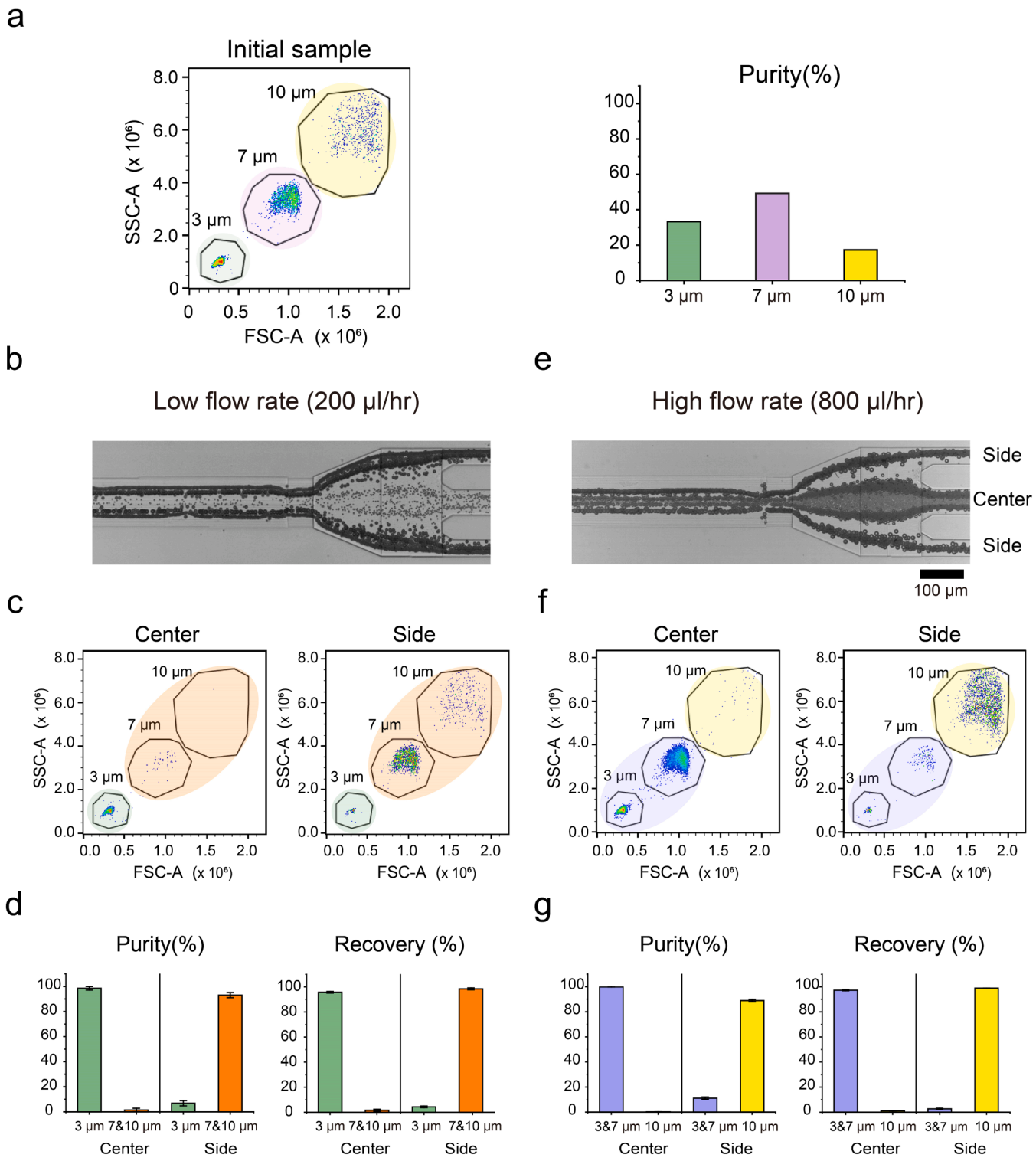

Fig. 3. Recovery and purity of different particle sizes collected at the various outlets. Different particles sizes (3 μm, 7 μm and 10 μm) were suspended in a 0.6% w/v PEO solution. (a) Forward-scatter area (FSC-A) vs side-scatter area (SSC-A) data show the composition of the initial particle mixture and the extracted purities of each particle population. (b, e) Image stacks show the various particle distributions at the side and center outlets at 200 and 800 μl/hr flow rates. (c, f) Scatter plots of SSC-A vs FSC-A show the distributions of 3 μm, 7 μm and 10 μm particles collected at the center and the side outlets at 200 and 800 μl/hr flow rates. (d, g) Bar graphs depict the purities and recoveries of the separated particle populations at 200 and 800 μl/hr flow rates, calculated from the scatter plots in (e) and (f). (d) At low flow rates (200 μl/hr), purities of 98.5% and 93.1% and recoveries of 95.7% and 98.4% were achieved for the 3 μm (collected at the center outlet) and for both 10 and 7 μm particles (collected at the side outlets) respectively. (g) At high flow rates (800 μl/hr), purities of 99.8% and 88.9% and recoveries of 97.3% and 98.9% were achieved for both 3 and 7 μm (collected at the centre outlet) and for 10 μm particles (collected at the side outlets) respectively. Standard deviations were extracted based on three different measurements.

exit via the center outlet, whilst the 7 μm and 10 μm particles travel close to the side walls and exit via the two side outlets. SSC-A vs FSC-A plots for particles collected at the center outlet indicate that most of the collected particles have a diameter of 3 μm (green), while particles collected at the side outlets are primarily 7 μm or 10 μm in diameter (Fig. 3**c**). Quantitative analysis yields a purity of 98.5 ± 1.4% for the 3 μm particles collected at the center outlet and 93.1 ± 2.1% for both the 10 μm and 7 μm particles collected at the side outlets (Fig. 3**d, left panel**). Additionally, these experimental conditions yielded a near complete recovery of the particles, namely 95.7 ± 0.7% for the 3 μm particles and 98.4 ± 0.8% for the 10 μm and 7 μm particles (Fig. 3**d, right panel**). At a flow rate of 800 μl/hr, the trajectory of 7 μm particles shifts from the side walls towards the channel centerline (Fig. 3**e**). This allowed 3 and 7 μm particles to be collected at the center outlet, while the 10 μm particles were collected at the two side outlets. Flow cytometry plots (SSC-A vs FSC-A) for sample collected at the center outlet showed two major clusters; one composed of 3 μm particles and the other of 7 μm particles (Fig. 3**f, blue**) while particles collected at the side outlets exhibited a single cluster composed of 10 μm particles (Fig. 3**f, yellow**). At high flow rates (800 μl/hr), the purities of particles collected at the center outlet were exceptionally high, reaching 99.8 ± 0.1% for both the 3 μm and 7 μm particle (Fig. 3**g, left**). Similarly, the purity of 10 μm particles collected at the side outlets was 88.9 ± 1%. Recoveries were also high, with 97.3 ± 0.4% for both the 3 μm and 7 μm particles collected at the center outlet and 98.9 ± 0.1% for the 10 μm particles collected at the side outlets (Fig. 3**g, right**).

3.4. Tunable separation of blood components and rare cells

We next investigated the utility of the triangular cross-section-shaped microfluidic channel in the size-selective separation of blood components (Fig. 4) and rare cells from whole blood (Fig. 5). The isolation of rare cells from whole blood is central to a number of important biological applications, most notably liquid biopsies [60,61]. Since the dimensions of the primary blood components, including platelets, RBCs and white blood cells, closely match the sizes of the 3 μm, 7 μm, and 10 μm particles used in earlier experiments, similar migration trajectories were expected when using the same experimental conditions. Accordingly, the initial blood sample entering the inlet and the sorted samples collected from the two outlets were analyzed by flow cytometry, counting at least 10,000 events. SSC-A vs FSC-A plots allowed blood components to be categorized based on granularity and size, demonstrating that platelets could be distinguished easily from both RBCs and WBCs [61,62] (Fig. 4**a**). Next, we reconstructed trajectories of each blood component within the microfluidic platform by stacking consecutive images acquired in the focusing zone (Fig. 4**b**). We observed patterns similar to those observed in the particle experiments (Fig. 3**b**). Notably, as the flow rate was increased from 200 μl/hr to 800 μl/hr, a clear transition of RBC focusing from the side walls (Fig. 4**b**) to the centerline (Fig. 4**f**) is observed, mirroring the behavior of the 7 μm particles. Furthermore, we successfully demonstrated the separation of platelets from a mixture of WBCs and RBCs at a flow rate of 200 μl/hr. Quantification of the different components collected at each outlet using flow cytometry revealed a notable increase in the purity of platelets from 6.1% in the initial blood sample (Figs. 4**a**) to 83.6 ± 4.8% in the sample collected at the center outlet (Fig. 4**d, left**). Platelet recovery was measured to be 70.8 ± 2.4% (Fig. 4**d, right**) and the RBC rejection percentage (from the side outlets) was found to be 96.1 ± 1.8%.

The fact that RBC trajectories move from the side to the center of the microfluidic channel, as the flow rate increases from 200 to 800 μl/hr, enables the efficient purification of WBCs (Fig. 4**f**). Scatter plots of violet SSC-A vs SSC-A report the distributions of WBCs and RBCs in the initial sample (Fig. 4**e**) and those collected at the center and side outlets (Fig. 4**g**). By tuning RBC focusing, the purity of WBCs increased from 0.1% in the initial sample (Fig. 4**e**), to 49.9 ± 10.6% (Fig. 4**h, left**) in the sample collected from the side outlets, with a corresponding recovery of 87.2 ± 6.4% (Fig. 4**h, right**). Monocytes (average diameters between 15 and 30 μm) and granulocytes (average diameters between 12 and15 μm) are larger than RBCs, while lymphocytes, constituting approximately 30% of WBCs, are similar in size to RBCs. Consequently, while the majority of WBCs could be effectively purified through size-based separation, some WBCs eluted through the center outlet. The percentage of rejected RBCs at the center outlet was 99.7 ± 0.2%.

Finally, we used our system to isolate rare cells from whole blood (HEK293T cells: blood cells: 1:10,000). Quantification using flow cytometry (Fig. 5**a**) allowed determination of both the purity and recovery of HEK293T cells in the processed fluid, which were found to be 26.3 ± 2.2% and 98.5 ± 0.6%, respectively (Fig. 5**b**). Here, the RBC rejection ratio was calculated at 99.9 ± 0.1%. Since HEK293T cells typically have diameters between 11 and 15 μm, they are generally larger than RBCs and thus can be efficiently separated and collected at the side outlet. Given that HEK293T cells typically have diameters between 14 and 16 μm, they are generally larger than RBCs and can be efficiently separated and collected at the side outlet. However, due to the size-based separation mechanism employed by the device, the purity of HEK293T cells in the sorted samples was slightly lower than that of WBCs. Nevertheless, our device demonstrates a 98.5% recovery rate, demonstrating its capability to enrich a diluted cell population from the vast majority of blood cells.

4. Discussion

We have introduced a novel microfluidic device, incorporating a triangular cross-section channel, to achieve efficient and tunable particle/cell focusing within a viscoelastic fluid. The system enables the efficient and label-free separation of micron-sized particles based on size. Initial calibration experiments were performed using particles with sizes that mimic the main components of blood. By balancing the hydrodynamic forces that arise from the asymmetric structure of the triangular cross-section microchannel, we achieved tunable size-based particle focusing through control of volumetric flow rates. Notably, the focusing behavior of mid-sized species could be selectively regulated by simply changing the applied flow rate. Leveraging this feature, we demonstrated efficient size-based separations of various blood components, including platelets and white blood cells. Furthermore, as proof of concept for liquid biopsies, we successfully demonstrated the separation of spiked HEK293T cells from a 10-fold diluted blood sample.

Microfluidic device performance can be evaluated using a number of parameters, including analytical throughput (flow rate), required blood dilution, purity and recovery, However, assessing the individual effects of each parameter on device performance is challenging, given the complex interdependencies that exist. For example, analytical throughput is defined as the number of cells that can be sorted within a given time period. Higher flow rates result in increased throughput, but they may also impact the focusing positions of particles, affecting both purity and separation efficiency. For example, Holzner et al. observed a correlation between cell focusing quality in non-Newtonian fluids and flow rate [63]. They found that at low flow rates cells exhibited a tight focus along the channel's centerline, whilst at higher flow rates, a defocusing effect emerged, attributed to the shear-thinning behavior of the carrier fluid. One of the most important features of our platform is its ability to achieve high recoveries even at low blood dilutions when compared to other approaches employing inertial or viscoelastic microfluidic devices. Unlike previous inertial studies that typically utilize highly diluted blood samples [18,19,43] (over 100-fold) or RBC-lysed blood to reduce cell-cell interactions [17,51,59], we employed only a 10-fold diluted blood sample. Despite this low blood dilution factor, our device achieved impressive recoveries for RBCs (98%) and WBCs (87%) as well as a notable WBC purity of 49%. To the best of our knowledge, only a few reports have demonstrated size-dependent particle/cell separations for low blood dilutions. In these cases, the blood dilution values were lower than the reported ones due to

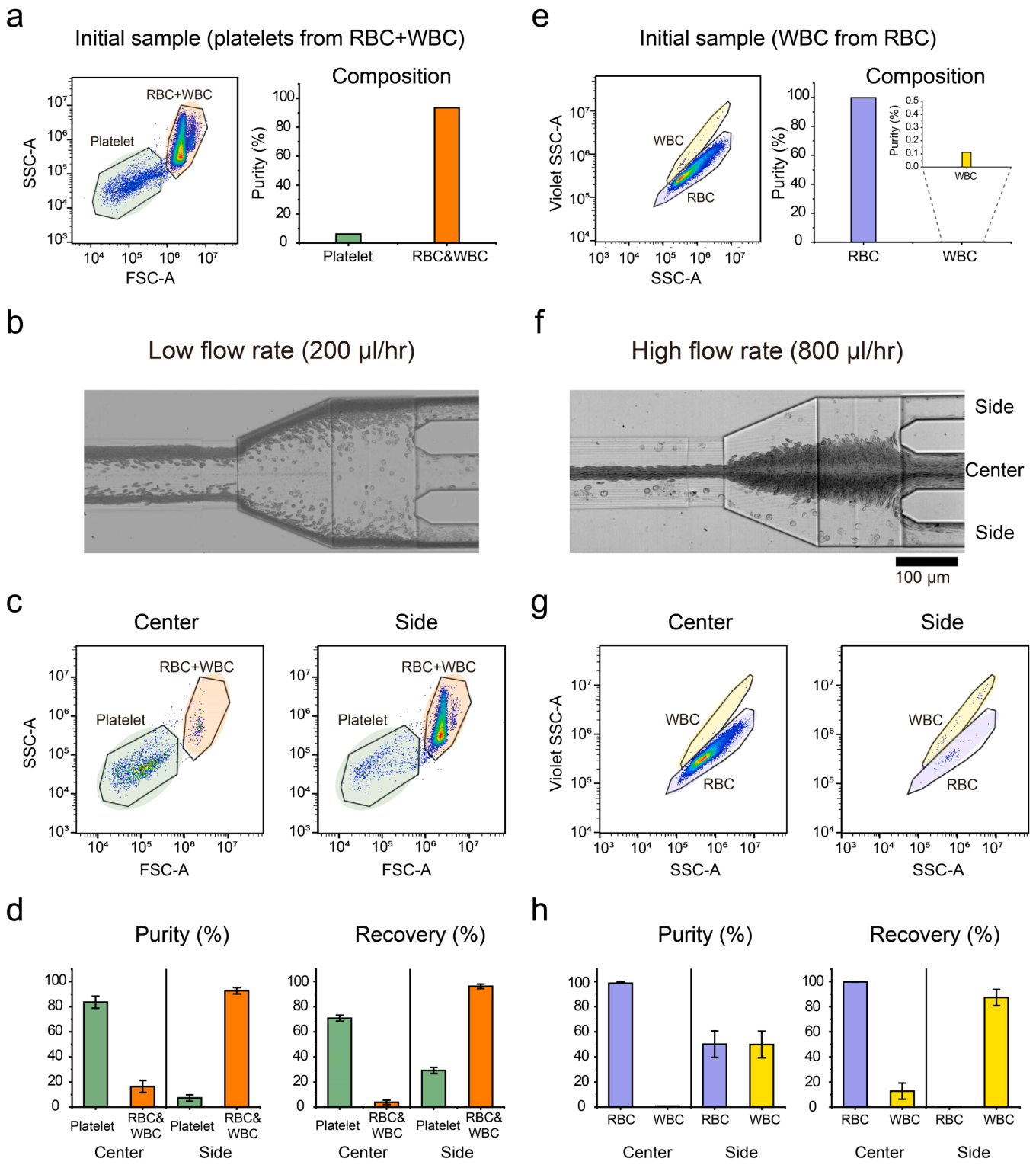

Fig. 4. Recovery and purity of blood components collected at various outlets. The blood sample was diluted 10-fold and suspended in a 0.3% w/v PEO solution. (a) A SSC-A vs FSC-A plot shows that platelets can be distinguished from both RBCs and WBCs. (b) Image stacks show the blood components distribution at the side and center outlets at a flow rate of 200 µl/hr. (c) Scatter plots of SSC-A vs FSC-A show the distributions of platelets at the center and the side outlets at a flow rate of 200 µl/hr. (d) Bar graphs depict the purities and recoveries of platelets from a mixture of WBCs and RBCs at a flow rate of 200 µl/hr. The purity of platelets increased from 6.1% in the initial blood sample (a) to 83.6% in the sample collected at the center outlet and the corresponding recovery was 70.8%. (e) A 405 nm side scatter area (violet SSC-A) vs 488 nm side scatter area (SSC-A) plot shows the distribution of WBCs in the initial sample. (f) An image stack at 800 µl/hr flow rate shows the distributions of WBCs and RBCs at the side and center outlets. (g) Scatter plots of violet SSC-A vs SSC-A show the distributions of WBCs and RBCs at the center and side outlets. (h) At high flow rates (800 µl/hr), WBCs were collected at the side outlets with a purity of 49.9% and a recovery of 87.2%.

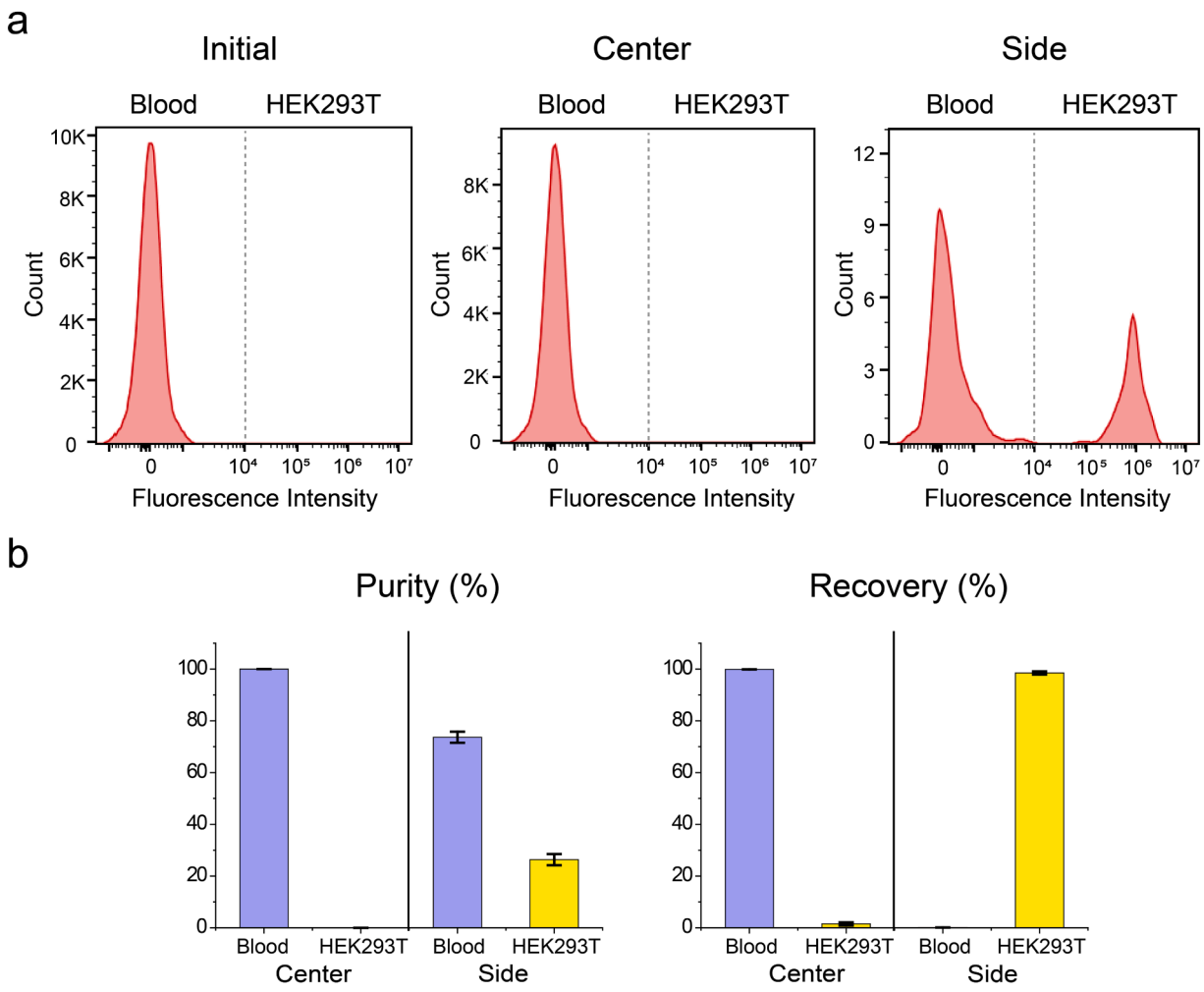

Fig. 5. Analysis of the separated rare cells (HEK293T cells) from a diluted blood sample. Cells were suspended in a 0.3% PEO solution and the sample flow rate was at 800 μl/hr. (a) Fluorescence intensity histograms extracted from flow cytometry measurements report the population of HEK293T cells in the initial blood sample and at the center and side outlets of the device. (b) Bar graphs depict the purities and recoveries of the separated HEK293T cell populations calculated from the scatter plots in (a).

the use of sheath flows. For instance, Zhou et al. [24] used a co-flow microfluidic system (whole blood sample flow was separated by a central stream of buffer) for separating different cell sizes in whole blood. However, due to the use of a sample-to-core ratio of 1:1, the blood sample was diluted 2-fold. In addition, this method demonstrated rather low WBC enrichment (2.6x) and purity (0.44%) values compared to those achieved in the current study, namely 490x and 49%, respectively. Additionally, Tian et al. [52] used a co-flow microfluidic system for label-free and size-selective isolation of CTCs using a dilute PEO (0.05%) solution as the core flow. They achieved a separation efficiency of 92.9% (equivalent to recovery) for WBCs from whole blood, which is comparable to that achieved in our case (87%). That said, the use of a sample-to-core ratio of 1:20 resulted in a dilution factor of 21. Finally, another noteworthy advantage of the current device is its capability for tunable separation of different-sized blood components, including WBCs and platelets from RBCs, as well as rare cells from other blood components. Separation is achieved on a single device without the need for additional sheath flows, complex device structures [22,64] or cascaded systems [65].

With the high recoveries and purities achieved on using device, we envision its application in a range of clinical scenarios that require the precise separation of various cell types from blood. One such potential application is the separation of other types of rare cells, such as fetal erythroblasts [66], which are present in maternal blood (one cell in 1 mL of maternal whole blood). This capability could pave the way for the development of a non-invasive method for prenatal diagnosis, revolutionizing the field of maternal-fetal medicine [67]. The passive nature of operation at low blood dilutions, coupled with the separation of different blood components highlights its potential as a powerful tool in various biomedical applications, such as liquid biopsies.

CRediT authorship contribution statement

Yingchao Meng: Resources, Methodology. **Stavros Stavrakis:** Writing – review & editing, Supervision, Project administration, Methodology, Investigation, Conceptualization. **Mahmut Kamil Aslan:** Visualization, Software, Data curation. **Andrew deMello:** Writing – review & editing, Supervision, Resources, Project administration, Funding acquisition, Conceptualization. **Eunhee Cho:** Writing – review & editing, Writing – original draft, Visualization, Methodology, Investigation, Formal analysis, Data curation, Conceptualization. **Jeong-ah Kim:** Writing – original draft, Visualization, Methodology, Investigation, Formal analysis, Data curation, Conceptualization.

Declaration of Competing Interest

Andrew deMello reports financial support, administrative support, article publishing charges, equipment, drugs, or supplies, statistical

analysis, travel, and writing assistance were provided by ETH Zurich. If there are other authors, they declare that they have no known competing financial interests or personal relationships that could have appeared to influence the work reported in this paper.

Data Availability

Data will be made available on request.

Acknowledgements

The authors acknowledge the support from Alessandra Stürchler and Dr Bogdan Mateescu for providing the fluorescently labeled HEK293T cell lines. This research was supported by ETH Zurich.

Appendix A. Supporting information

Supplementary data associated with this article can be found in the online version at doi:10.1016/j.snb.2024.135892.

References

[1] G. Gharib, I. Butun, Z. Muganli, G. Kozalak, I. Namli, S.S. Sarraf, et al., Biomedical applications of microfluidic devices: a review, Biosensors 12 (2022).
[2] S. Zhang, Y. Wang, P. Onck, J. den Toonder, A concise review of microfluidic particle manipulation methods, Microfluid. Nanofluidics 24 (2020) 24.
[3] D.R. Gossett, W.M. Weaver, A.J. Mach, S.C. Hur, H.T.K. Tse, W. Lee, et al., Label-free cell separation and sorting in microfluidic systems, Anal. Bioanal. Chem. 397 (2010) 3249–3267.
[4] A. Munaz, M.J.A. Shiddiky, N.-T. Nguyen, Recent advances and current challenges in magnetophoresis based micro magnetofluidics, Biomicrofluidics 12 (2018) 031501.
[5] T. Laurell, F. Petersson, A. Nilsson, Chip integrated strategies for acoustic separation and manipulation of cells and particles, Chem. Soc. Rev. 36 (2007) 492–506.
[6] P.R.C. Gascoyne, J. Vykoukal, Particle separation by dielectrophoresis, Electrophoresis 23 (2002) 1973–1983.
[7] A.T. Ohta, P. Chiou, H.L. Phan, S.W. Sherwood, J.M. Yang, A.N.K. Lau, et al., Optically controlled cell discrimination and trapping using optoelectronic tweezers, IEEE J. Sel. Top. Quantum Electron 13 (2007) 235–243.
[8] J. Takagi, M. Yamada, M. Yasuda, M. Seki, Continuous particle separation in a microchannel having asymmetrically arranged multiple branches, Lab Chip 5 (2005) 778–784.
[9] H.M. Ji, V. Samper, Y. Chen, C.K. Heng, T.M. Lim, L. Yobas, Silicon-based microfilters for whole blood cell separation, Biomed. Micro 10 (2008) 251–257.
[10] D.W. Inglis, Efficient microfluidic particle separation arrays, Appl. Phys. Lett. 94 (2009) 013510.
[11] M. Yamada, M. Seki, Hydrodynamic filtration for on-chip particle concentration and classification utilizing microfluidics, Lab Chip 5 (2005) 1233–1239.
[12] H. Amini, W. Lee, D. Di Carlo, Inertial microfluidic physics, Lab Chip 14 (2014) 2739–2761.
[13] J. Zhou, I. Papautsky, Viscoelastic microfluidics: progress and challenges, Microsyst. Nanoeng. 6 (2020) 113.
[14] D. Stoecklein, D. Di Carlo, Nonlinear Microfluidics, Anal. Chem. 91 (2019) 296–314.
[15] X. Lu, C. Liu, G. Hu, X. Xuan, Particle manipulations in non-Newtonian microfluidics: a review, J. Colloid Interface Sci. 500 (2017) 182–201.
[16] D. Di Carlo, Inertial microfluidics, Lab Chip 9 (2009) 3038–3046.
[17] A. Abdulla, W. Liu, A. Gholamipour-Shirazi, J. Sun, X. Ding, High-Throughput isolation of circulating tumor cells using cascaded inertial focusing microfluidic channel, Anal. Chem. 90 (2018) 4397–4405.
[18] Y. Gou, S. Zhang, C. Sun, P. Wang, Z. You, Y. Yalikun, et al., Sheathless inertial focusing chip combining a spiral channel with periodic expansion structures for efficient and stable particle sorting, Anal. Chem. 92 (2020) 1833–1841.
[19] Y. Zhou, Z. Ma, Y. Ai, Sheathless inertial cell focusing and sorting with serial reverse wavy channel structures, Microsyst. Nanoeng. 4 (2018) 5.
[20] J. Shi, B. Wu, S. Li, J. Song, B. Song, W.F. Lu, Shear stress analysis and its effects on cell viability and cell proliferation in drop-on-demand bioprinting, Biomed. Phys. Eng. Express 4 (2018) 045028.
[21] T. Suwannaphan, A. Pimpin, W. Srituravanich, W. Jeamsaksiri, W. Sripumkhai, D. Ketpun, et al., Investigation of shear stress and cell survival in a microfluidic chip for a single cell study, 2015 8th Biomed. Eng. Int. Conf. (BMEiCON), 2015, pp. 1-5.
[22] J. Nam, J. Yoon, J. Kim, W.S. Jang, C.S. Lim, Continuous erythrocyte removal and leukocyte separation from whole blood based on viscoelastic cell focusing and the margination phenomenon, J. Chromatogr. A 1595 (2019) 230–239.
[23] J. Zhou, C. Tu, Y. Liang, B. Huang, Y. Fang, X. Liang, et al., Isolation of cells from whole blood using shear-induced diffusion, Sci. Rep. 8 (2018) 9411.
[24] J. Zhou, I. Papautsky, Size-dependent enrichment of leukocytes from undiluted whole blood using shear-induced diffusion, Lab Chip 19 (2019) 3416–3426.
[25] R. Mohammadi, M. Asghari, M. Colombo, Z. Vaezi, D.A. Richards, S. Stavrakis, et al., Hybrid Microfluidic Device for High Throughput Isolation of Cells Using Aptamer Functionalized Diatom Frustules, Chimia 76 (2022) 661–668.
[26] G. Holzner, B. Mateescu, D. van Leeuwen, G. Cereghetti, R. Dechant, S. Stavrakis, et al., High-throughput multiparametric imaging flow cytometry: toward diffraction-limited sub-cellular detection and monitoring of sub-cellular processes, Cell Rep. 34 (2021) 108824.
[27] H. Lim, S.M. Back, M.H. Hwang, D.H. Lee, H. Choi, J. Nam, Sheathless High-Throughput Circulating Tumor Cell Separation Using Viscoelastic non-Newtonian Fluid, Micromachines 10 (2019) 462.
[28] J.Y. Kim, S.W. Ahn, S.S. Lee, J.M. Kim, Lateral migration and focusing of colloidal particles and DNA molecules under viscoelastic flow, Lab Chip 12 (2012) 2807–2814.
[29] C. Liu, B. Ding, C. Xue, Y. Tian, G. Hu, J. Sun, Sheathless focusing and separation of diverse nanoparticles in viscoelastic solutions with minimized shear thinning, Anal. Chem. 88 (2016) 12547–12553.
[30] Y. Zhou, Z. Ma, M. Tayebi, Y. Ai, Submicron particle focusing and exosome sorting by wavy microchannel structures within viscoelastic fluids, Anal. Chem. 91 (2019) 4577–4584.
[31] M. Asghari, X. Cao, B. Mateescu, D. van Leeuwen, M.K. Aslan, S. Stavrakis, et al., Oscillatory viscoelastic microfluidics for efficient focusing and separation of nanoscale species, ACS Nano 14 (2020) 422–433.
[32] Y. Meng, M. Asghari, M.K. Aslan, A. Yilmaz, B. Mateescu, S. Stavrakis, et al., Microfluidics for extracellular vesicle separation and mimetic synthesis: recent advances and future perspectives, Chem. Eng. J. 404 (2021) 126110.
[33] J. Zhou, P. Mukherjee, H. Gao, Q. Luan, I. Papautsky, Label-free microfluidic sorting of microparticles, APL Bioeng. 3 (2019) 041504.
[34] I. De Santo, G. D'Avino, G. Romeo, F. Greco, P.A. Netti, P.L. Maffettone, Microfluidic lagrangian trap for brownian particles: three-dimensional focusing down to the nanoscale, Phys. Rev. Appl. 2 (2014) 064001.
[35] A.T. Ciftlik, M. Ettori, M.A.M. Gijs, High throughput-per-footprint inertial focusing, Small 9 (2013) 2764–2773.
[36] D. Li, X. Lu, X. Xuan, Viscoelastic separation of particles by size in straight rectangular microchannels: a parametric study for a refined understanding, Anal. Chem. 88 (2016) 12303–12309.
[37] D. Di Carlo, J.F. Edd, K.J. Humphry, H.A. Stone, M. Toner, Particle segregation and dynamics in confined flows, Phys. Rev. Lett. 102 (2009) 094503.
[38] S.C. Hur, S.-E. Choi, S. Kwon, D.D. Carlo, Inertial focusing of non-spherical microparticles, Appl. Phys. Lett. 99 (2011) 044101.
[39] M.E. Warkiani, G. Guan, K.B. Luan, W.C. Lee, A.A.S. Bhagat, P. Kant Chaudhuri, et al., Slanted spiral microfluidics for the ultra-fast, label-free isolation of circulating tumor cells, Lab Chip 14 (2014) 128–137.
[40] J. Kim, J. Lee, C. Wu, S. Nam, D. Di Carlo, W. Lee, Inertial focusing in non-rectangular cross-section microchannels and manipulation of accessible focusing positions, Lab Chip 16 (2016) 992–1001.
[41] P. Mukherjee, X. Wang, J. Zhou, I. Papautsky, Single stream inertial focusing in low aspect-ratio triangular microchannels, Lab Chip 19 (2019) 147–157.
[42] J.A. Kim, A. Kommajosula, Y.H. Choi, J.R. Lee, E.C. Jeon, B. Ganapathysubramanian, et al., Inertial focusing in triangular microchannels with various apex angles, Biomicrofluidics 14 (2020) 024105.
[43] J.A. Kim, J.R. Lee, T.J. Je, E.C. Jeon, W. Lee, Size-dependent inertial focusing position shift and particle separations in triangular microchannels, Anal. Chem. 90 (2018) 1827–1835.
[44] J.Y. Kwon, T. Kim, J. Kim, Y. Cho, Particle focusing under newtonian and viscoelastic flow in a straight rhombic microchannel, Micromachines 11 (2020) 998.
[45] M.A. Raoufi, A. Mashhadian, H. Niazmand, M. Asadnia, A. Razmjou, M. E. Warkiani, Experimental and numerical study of elasto-inertial focusing in straight channels, Biomicrofluidics 13 (2019) 034103.
[46] M.A. Raoufi, S. Razavi Bazaz, H. Niazmand, O. Rouhi, M. Asadnia, A. Razmjou, et al., Fabrication of unconventional inertial microfluidic channels using wax 3D printing, Soft Matter 16 (2020) 2448–2459.
[47] J. Nam, H. Lim, D. Kim, H. Jung, S. Shin, Continuous separation of microparticles in a microfluidic channel via the elasto-inertial effect of non-Newtonian fluid, Lab Chip 12 (2012) 1347–1354.
[48] S. Yang, J.Y. Kim, S.J. Lee, S.S. Lee, J.M. Kim, Sheathless elasto-inertial particle focusing and continuous separation in a straight rectangular microchannel, Lab Chip 11 (2011) 266–273.
[49] D. Yuan, J. Zhang, R. Sluyter, Q. Zhao, S. Yan, G. Alici, et al., Continuous plasma extraction under viscoelastic fluid in a straight channel with asymmetrical expansion–contraction cavity arrays, Lab Chip 16 (2016) 3919–3928.
[50] J. Nam, W.S. Jang, D.H. Hong, C.S. Lim, Viscoelastic Separation and Concentration of Fungi from Blood for Highly Sensitive Molecular Diagnostics, Sci. Rep. 9 (2019) 3067.
[51] M.E. Warkiani, B.L. Khoo, D.S.W. Tan, A.A.S. Bhagat, W.-T. Lim, Y.S. Yap, et al., An ultra-high-throughput spiral microfluidic biochip for the enrichment of circulating tumor cells, Analyst 139 (2014) 3245–3255.
[52] F. Tian, L. Cai, J. Chang, S. Li, C. Liu, T. Li, et al., Label-free isolation of rare tumor cells from untreated whole blood by interfacial viscoelastic microfluidics, Lab Chip 18 (2018) 3436–3445.
[53] C. Liu, C. Xue, X. Chen, L. Shan, Y. Tian, G. Hu, Size-based separation of particles and cells utilizing viscoelastic effects in straight microchannels, Anal. Chem. 87 (2015) 6041–6048.
[54] A. Bogseth, J. Zhou, I. Papautsky, Evaluation of performance and tunability of a co-flow inertial microfluidic device, Micromachines 11 (2020).

[55] W. Tang, S. Zhu, D. Jiang, L. Zhu, J. Yang, N. Xiang, Channel innovations for inertial microfluidics, Lab Chip 20 (2020) 3485–3502.
[56] J. Zhang, D. Yuan, Q. Zhao, S. Yan, S.-Y. Tang, S.H. Tan, et al., Tunable particle separation in a hybrid dielectrophoresis (DEP)- inertial microfluidic device, Sens. Actuators B Chem. 267 (2018) 14–25.
[57] V. Ost, J. Neukammer, H. Rinneberg, Flow cytometric differentiation of erythrocytes and leukocytes in dilute whole blood by light scattering, Cytometry 32 (1998) 191–197.
[58] K. Ebagninin, A. Benchabone, K. Bekkour, Rheological characterization of poly (ethylene oxide) solutions of different molecular weights, J. Colloid Interface Sci. 336 (2009) 360–367.
[59] B.L. Khoo, M.E. Warkiani, D.S. Tan, A.A. Bhagat, D. Irwin, D.P. Lau, et al., Clinical validation of an ultra high-throughput spiral microfluidics for the detection and enrichment of viable circulating tumor cells, PLoS One 9 (2014) e99409.
[60] K.B. Shanmugasundaram, J. Li, A.I. Sina, A. Wuethrich, M. Trau, Toward precision oncology: SERS microfluidic systems for multiplex biomarker analysis in liquid biopsy, Mater. Adv. 3 (2022) 1459–1471.
[61] N. Soda, K. Clack, M.J.A. Shiddiky, Recent advances in liquid biopsy technologies for cancer biomarker detection, Sens. Diagn. 1 (2022) 343–375.
[62] L.G. Rico, R. Salvia, M.D. Ward, J.A. Bradford, J. Petriz, Flow-cytometry-based protocols for human blood/marrow immunophenotyping with minimal sample perturbation, STAR Protoc. 2 (2021) 100883.
[63] G. Holzner, S. Stavrakis, A. deMello, Elasto-inertial focusing of mammalian cells and bacteria using low molecular, low viscosity PEO solutions, Anal. Chem. 89 (2017) 11653–11663.
[64] D.H. Kuan, C.C. Wu, W.Y. Su, N.T. Huang, A microfluidic device for simultaneous extraction of plasma, red blood cells, and on-chip white blood cell trapping, Sci. Rep. 8 (2018) 15345.
[65] J.K.S. Tan, S.Y. Park, H.L. Leo, S. Kim, Continuous separation of white blood cells from whole blood using viscoelastic effects, IEEE Trans. Biomed. Circuits Syst. 11 (2017) 1431–1437.
[66] L.H. Ripudaman Singh, Katarina Ravn, Ida Vogel, Olav Bjørn Petersen, Niels Uldbjerg, Palle Schelde, Fetal cells in maternal blood for prenatal diagnosis: a love story rekindled, Biomark. Med 11 (2017) 705–710.
[67] C. Troeger, X.Y. Zhong, R. Burgemeister, S. Minderer, S. Tercanli, W. Holzgreve, et al., Approximately half of the erythroblasts in maternal blood are of fetal origin, Mol. Hum. Reprod. 5 (1999) 1162–1165.

Andrew deMello received his bachelor's degree in chemistry from Imperial College London. After completing his PhD in MolecularPhotophysics atthe same university, he took up a postdoctoral fellowship at the University of California, Berkeley working withProfessor Richard Mathies on early microfluidic systems for DNA analysis. After returning to the UK, Andrew became Professor of Chemical Nanosciences at Imperial College London. He moved to ETH Zurich in 2011, where he now holds the Chair of Biochemical Engineering. His group's research interests lie in the general area of microfluidics and nanoscale science. Primary specializations include the development of microfluidic devices for high-throughput biological and chemical experimentation, ultrasensitive optical detection techniques and the exploitation of point-of-care diagnostic technologies. Andrew has given approximately 450 invited lectures (including 100 plenary or keynote lectures) describing these activities and has published 400 papers in the peer-reviewed literature.